Simulation of online selection for $B^0\_d \to K^{*0}\gamma$ and $B^0\_s \to \phi\gamma$ decays at ATLAS experiment

S. Viret, F. Ohlsson-Malek, M. Smizanska

December 18th, 2004.

Simulation of online selection for $B_d^0 \to K^{*0}\gamma$ and $B_s^0 \to \phi\gamma$ decays at ATLAS experiment

S. Viret[a], F. Ohlsson-Malek[a], M. Smizanska[b]

[a] Laboratoire de Physique Subatomique et de Cosmologie, Université J. Fourier, IN2P3-CNRS, Grenoble, France
[b] University of Lancaster, Lancaster, UK

Abstract

The observation potential of the $B_d^0 \to K^{*0}\gamma$ and $B_s^0 \to \phi\gamma$ decays with the ATLAS detector at the LHC is described in this paper. Radiative B decays involve $b \to s$ or $b \to d$ transitions which occur only at loop-level in the Standard-Model (SM) where they are sensitive to the CKM matrix elements $|V_{ts}|$ and $|V_{td}|$. They come with small branching ratios and provide a probe of indirect new physics effects.

This paper shows the feasibility of a radiative B decays trigger in ATLAS. This study is based on a simulation of the ATLAS detector response at $2 \times 10^{33}\mathrm{cm}^{-2}\mathrm{s}^{-1}$ luminosity. We show that for one year about 10000 $B_d^0 \to K^{*0}\gamma$ and 3300 $B_s^0 \to \phi\gamma$ events can be selected by trigger, and that the signal to background ratio can be improved from 10^{-7} before LVL1 to about 10^{-2} after LVL2 and event filter. Because the online reconstruction tools were not available, the trigger analysis were emulated using the offline software.

1 Introduction

Flavor-changing neutral-current involving $b \to s$ or $b \to d$ transitions occur only at loop-level in the Standard-Model (SM). Therefore they come with small branching ratios and thus provide a probe of indirect new physics effects.

Radiative B decays, like $B_d^0 \to K^{*0}\gamma$ and $B_s^0 \to \phi\gamma$, are the most "frequent" rare B channels. Within the SM, these decays are sensitive to the CKM matrix elements $|V_{ts}|$ and $|V_{td}|$. Moreover, it has been shown ([1],[2]) that new physics contributions could enhance largely $\mathcal{C}P$ or isospin violation in this sector.

Since the first observation of $B_d \to K^{*0}\gamma$ in 1993 [3], inclusive and exclusive measurements of radiative B at LEP and B factories provided new informations about branching ratios, $\mathcal{C}P$ and isospin asymmetries. However, precise asymmetries measurement still suffer from large experimental uncertainties [4], and B_s sector will remain inaccessible to BaBar or BELLE.

LHC will provide high statistics in all the rare B decays area, but the background will also largely increase.

This note shows that a radiative B decays trigger is feasible in ATLAS. This study is based on a simulation of the ATLAS detector response at low luminosity of $2 \times 10^{33}\mathrm{cm}^{-2}\mathrm{s}^{-1}$. The online selection scheme is described in section 3. In section 4, a preliminary significance estimate shows that we will be able to observe clearly $B_s^0 \to \phi\gamma$ and $B_d^0 \to K^{*0}\gamma$ after only one year at low luminosity at ATLAS.

2 Data samples

The Monte Carlo events that have been used in this study are described in table 1. These events have been produced within the Data-Challenges framework: DC1 [5]. Pythia 6.2 [6] interfaced with PythiaBModule [7] has been used at the generation level.

	Generation		**Simulation**		**Reconstruction**	
Process	Stat.	Release	Stat.	Release	Stat.	Release
$b\bar{b} \to \mu_6 X + Pile-Up$					40000	7.0.2
$B_d \to K^{*0}_{\to K^+\pi^-}\gamma$	30000	7.5.0	30000	6.0.2	30000	7.0.2
$B_s \to \phi_{\to K^+K^-}\gamma$	30000	7.5.0	30000	6.0.2	15000	7.0.2

Table 1: *Data samples produced for the study.*

The Initial Layout geometry [9] was used at the simulation level and the pile-up at low luminosity was added to the background sample. The electronic noise was taken into account in the calorimeter at the reconstruction level.

2.1 Signal generation

At the generation level, b-quark pairs were produced in pp-collisions at $\sqrt{s} = 14$ TeV either directly via the lowest order process, or via gluon splitting or flavor excitation. Only events passing the ATLAS trigger LVL1 requirements for B hadrons (a muon with a $p_{\mathrm{T}} > 6$ GeV/c and $|\eta| < 2.5$) were retained[1].

A decay model [10], taking into account the non-uniform angular distributions of the ϕ and the K^{*0} decay products, was developed and interfaced with Pythia in order to produce the

[1]Throughout this paper, the symbol p_{T} is used for the transverse momentum, computed in the laboratory frame, with respect to the beam direction, and η for the pseudorapidity.

signal events (for more information, see [11]). Only events with K^{*0} decaying to $K^+\pi^-$ and ϕ decaying to K^+K^- were considered in our study.

A full GEANT3-based modelization of the ATLAS detector was used for the simulation. Pile-up was not included in the signal events.

As the muon chambers were not included at the reconstruction level, LVL1 trigger muon has been selected using the MC truth. The results presented throughout this paper assume a 85% identification efficiency for the muon.

2.2 Background definition

The generic background is constituted by $pp \to \mu_6 X$ events. The composition of this process is given in table 2. All background cross sections in table 2 are related only to the events in which muon passed a sharp $p_{\mathrm{T}} > 6$ GeV/c cut. This approximation is relevant to the situation after LVL2 muon reconstruction. The situation after LVL1 is discussed in the section 3.1. Secondary muons, coming from pions and kaons decays, are constituting the majority of the events (about 60%). Prompt muons, coming from b or c quarks decays, come with a proportion of 25% and 12% respectively. According to earlier study [9], combining the inner detector and muon system information, about 78% of the secondary muons can be rejected at the beginning of LVL2.

Process	**Cross-section (in $\mu barn$)**
$pp \to b\bar{b} \to \mu_6 X$	2.3
$pp \to c\bar{c} \to \mu_6 X$	1.1
$pp \to (K, \pi) \to \mu_6 X$	5.4

Table 2: *Generic $pp \to \mu_6 X$ background composition ($p_T(\mu) > 6$ GeV/c)*[9].

As $pp \to c\bar{c} \to \mu_6 X$ events were not yet produced, they have been included to the $pp \to b\bar{b} \to \mu_6 X$ cross-section. The secondary muons effect was also taken into account artificially by adding 20% of their global cross-section (the proportion of secondary muons passing the LVL2 muon confirmation) to $b\bar{b}$'s ones.

Finally, only $pp \to b\bar{b} \to \mu_6 X$ events have been produced. However, in order to take into account the other effects, the background cross-section within ATLAS LVL1 acceptance, σ_{bg}, has been overestimated as follows:

$$\sigma_{bg} = \sigma(pp \to b\bar{b} \to \mu_6 X) + \sigma(pp \to c\bar{c} \to \mu_6 X) + 0.2\sigma(pp \to (K, \pi) \to \mu_6 X) = 4.5\ \mu barn. \quad (2.1)$$

However, as each contribution will be quite well identified at the end of the online selection, we could reasonably consider this value as a pessimistic upper limit.

2.3 Irreducible background

Irreducible background is constituted by the decays which are kinematically very close to the signal. Their branching fractions are comparable to the signal one, consequently they are not taken into account in the general background sample. For $B_d \to K^{*0}\gamma$ these background modes are the following: $\boldsymbol{B_d \to K^{*0}\pi^0}$, $\boldsymbol{B_s \to K^{*0}\gamma}$, $\boldsymbol{B_d \to \rho\gamma}$ and $\boldsymbol{B_d \to K_1^{*0}(1270)\gamma}$.

As shown in table 3, all these modes have production rates which are at least 10 times smaller than $B_d \to K^{*0}\gamma$. For example, the $B_d \to K^{*0}\pi^0$ experimental branching fraction limit is $Br(B_d \to K^{*0}\pi^0) < 3.6 \times 10^{-6}$ [12].

In addition, further cuts can be applied in order to improve this limit (for example γ/π^0 separation in $B_d \to K^{*0}\pi^0$ case).

A complete analysis of the different modes is found in [13]. It justifies the fact that we only use the generic $b\bar{b} \to \mu_6 X$ sample for the background study at trigger level.

Decay channel	**Problem**	$\frac{N_{prod}^{signal}}{N_{prod}^{decay}}$
$B_d \to K^{*0}\pi^0$	π/γ identification	> 10
$B_s \to K^{*0}\gamma$	B_s/B_d identification	> 40
$B_d \to \rho\gamma$	ρ/K^{*0} identification	> 10
$B_d \to K_1^{*0}(1270)\gamma$	K_1^{*0}/K^{*0} identification	> 25

Table 3: *Summary of the specific background channels for* $B_d \to K^{*0}\gamma$.

We have presented the $B_d \to K^{*0}\gamma$ case only, but it is straightforward to extend this analysis to $B_s \to \phi\gamma$. Moreover, only $\boldsymbol{B_d \to \phi\gamma}$ and $\boldsymbol{B_s \to \phi\pi^0}$ have to be considered in this case.

2.4 Cross section and event rate

The $b\bar{b}$ cross section within ATLAS LVL1 acceptance has been estimated by Pythia:

$$\sigma_{b\bar{b}}^{Pythia} = \sigma(pp \to b\bar{b} \to \mu_6 X) = 2.3\ \mu barn\ [14].$$

For the signal, we get:

$$\sigma_{signal}^{Pythia} = \sigma\left(pp(14\ TeV) \to \left\{ \begin{array}{c} b \to \mu X \\ \bar{b} \to B \end{array} \right.\right) \times \underbrace{Br(B \to K^{*0}(\phi)\gamma)}_{=1} \times \underbrace{Br(K^{*0}(\phi) \to ab)}_{\left\{ \begin{array}{c} Br(K^{*0} \to K^+\pi^-) = \frac{2}{3} \\ Br(\phi \to K^+K^-) = 0.489 \end{array} \right.} \tag{2.2}$$

The B meson is forced to decay to $B \to K^{*0}(\phi)\gamma$. For this reason we have $Br(B \to K^{*0}(\phi)\gamma) = 1$. The values obtained with Pythia are the following:

$$\sigma_{signal}^{Pythia} = \left\{ \begin{array}{lll} 0.147\ \mu b & \text{for} & B_d \to K^{*0}\gamma \\ 0.036\ \mu b & \text{for} & B_s \to \phi\gamma \end{array} \right. . \tag{2.3}$$

We then can calculate the event rate for the observed signal in the ATLAS detector acceptance:

$$N_{signal} = 2 \times \sigma_{signal}^{Pythia} \times Br(B \to K^{*0}(\phi)\gamma) \times \mathcal{L}_{inst}\ , \tag{2.4}$$

where $\mathcal{L}_{inst} = 2 \times 10^{33} cm^{-2} s^{-1}$. The factor 2 is due to the fact that we generate only B mesons while we have to take into account the $\bar{B}$. If we admit that $Br(B_d \to K^{*0}\gamma) \approx Br(B_s \to \phi\gamma) = (4.17 \pm 0.23) \times 10^{-5}$ [4], we obtain at low luminosity:

$$N_{signal} = \left\{ \begin{array}{ll} 12200 \pm 700 & B_d \to K^{*0}\gamma/fb^{-1} \\ 3000 \pm 200 & B_s \to \phi\gamma/fb^{-1} \end{array} \right. . \tag{2.5}$$

The background rate is of the order of 9000 events per second, i.e. 4.5×10^9 events per fb^{-1}! Therefore, it is clear that some cuts should be performed to overcome this background at the trigger level. These cuts are presented in the next section.

3 Radiative B decays selection

The main goal of the study is to develop a radiative penguin trigger strategy for ATLAS. For this group of channels we are required to reach an output rate of the order of 10 Hz at the level 2 (LVL2) and 1 Hz after the Event Filter (EF). The three steps of the proposed strategy are the following:

- At **Level 1**, we look for a muon in the spectrometer together with an isolated Region Of Interest (ROI) in the electromagnetic calorimeter (ECal).
- At **Level 2**, we first perform a photon identification in ECal ROI, then define an inner detector (ID) ROI matching the ECal one in order to select track pairs.
- At **Level 3**, we perform a complete event reconstruction.

It should be noticed that the work presented below was done using the offline software. However, the cuts were taking into account timing and resolution constraints based on earlier studies of B-trigger group [9].

3.1 Level 1

After LVL1 and applying the 6 GeV/c single-muon trigger, the expected event rate would be as high as 22 kHz at luminosity 10^{33} cm$-$2 s$-$1 [8]. However, this value is not relevant in our case, as we require both electron and muon signature at LVL1, thus reducing substantially the LVL1 output rate [9].

One of the most critical parameters is E_T: the transverse energy threshold of this ROI. The lower the threshold is set, the higher is our chance to select the photon we are looking for. However, a low threshold will increase ROI multiplicity which will be difficult to handle correctly at LVL2. We thus choose 5 GeV as a lower limit for the E_T threshold value. For the muon, we start from the usual ATLAS LVL1 requirement: $p_T > 6$ GeV/c.

As a summary we have at LVL1:

- Muon with $p_T > 6$ GeV/c and $|\eta| < 2.5$.
- At least one isolated ECal ROI with $E_T > 5$ GeV and $|\eta| < 2.5$.

As we are not using LVL1 trigger software, the results presented below are obtained with 3×3 *offline-like* clusters instead of 8×8 ECal ROIs. Indeed we consider, as a first approximation, that the 3×3 cluster and the 8×8 ROI (η, ϕ) barycenters are identical. This argument is justified by the fact that we are at low luminosity, with a low probability to have more than one shower in a 8×8 ECal ROI.

The search for $K^{*0}(\phi)$ decay products in the inner detector will be done at LVL2, in an ROI centered around the ECal ROI. In order to define the inner detector ROI dimensions, the ECAL ROI coordinates are compared to those of the two ID tracks we are looking for, coming from $K^{*0}(\phi)$ decay products. To this end we introduce the following variables:

$$\begin{cases} \Delta_\phi = \phi_{track} - \phi_\gamma \\ \Delta_\eta = \eta_{track} - \eta_\gamma \end{cases} . \tag{3.1}$$

Δ_ϕ and Δ_η are represented on figs.1 and 2 respectively. Histograms values are normalized to 1. For the background, all the possible combinations were considered. The peaks at $\Delta_\phi = \Delta_\eta = 0$ values are due to electrons. The area defined by the values $(\Delta_\phi, \Delta_\eta) = (\pi, 2)$ contains most of the signal events. Consequently, the transition between LVL1 and LVL2 works as follows:

1. For timing reasons, if there is more than one ECal ROI, the one with the highest E_T is chosen.
2. A $((\Delta_\phi, \Delta_\eta) = (\pi, 2))$ ID ROI, centered on the Ecal one, is prepared for the LVL2.

3.2 Level 2

Apart from the muon confirmation which will not be discussed here, LVL2 is divided into two parts:

1. ECal ROI full reconstruction and photon identification.
2. Track pairs search in the previously defined ID ROI.

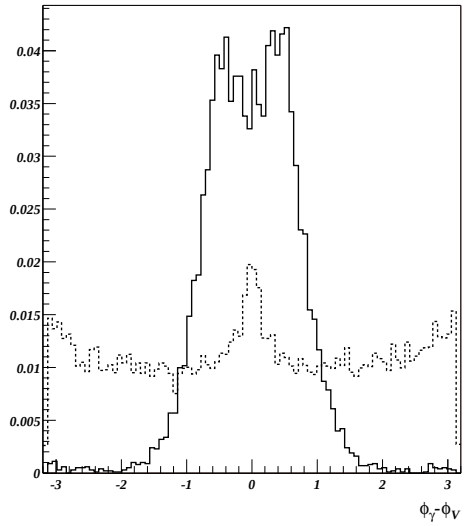

Figure 1: Δ_ϕ*: the black line corresponds to the signal, the dashed line to the background.*

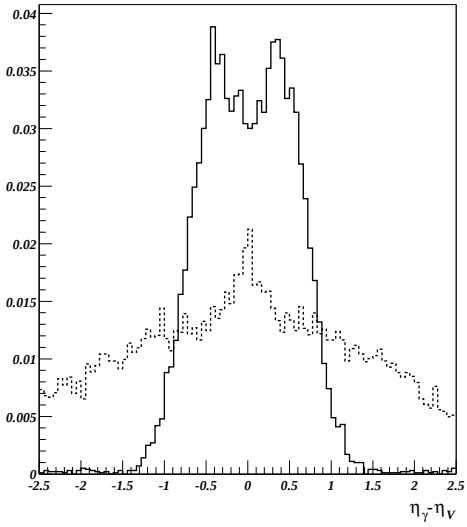

Figure 2: Δ_η*: the black line corresponds to the signal, the dashed line to the background.*

3.2.1 Photon identification in the calorimeter

Two kind of questions were studied for the photon identification in the calorimeter:

- Study the particles shower shapes and perform the necessary cuts to clean the data samples from unwanted background.
- Find a good way to reject the π^0.

Shower profiles provide interesting features as, at equal energy, a hadronic shower shape is wider and deeper than an electromagnetic one.

The fraction of energy deposited in the hadronic calorimeter (HCal) first sampling describes the shower longitudinal development. It can be expressed as :

$$P_1 = \frac{E_T^{Hcal^1}}{E_T^{Ecal}} \ . \tag{3.2}$$

The distribution of the parameter P_1 is shown on figure 3 for the signal ($B_s \to \phi\gamma$ and $B_d \to K^{*0}\gamma$) in full line and the background in dashed line. Both figures are normalized to 1. The mean values extracted from these distributions are $\langle P_1 \rangle_{signal} = 1.2\%$ and $\langle P_1 \rangle_{background} = 2.0\%$. A non-negligible background fraction can be eliminated using the following cut:

$$P_1 < 2.0 \ \% \ . \tag{3.3}$$

For the lateral shower development, we can define three parameters. The first interesting one is the shower width, computed on 21 strips. It is shown on figure 4 for the signal (full line) and the background (dashed line):

$$P_2 = W_{21} \ . \tag{3.4}$$

A clear difference is observed between the signal and the background shape and the mean values obtained are: $\langle P_2 \rangle_{signal} = 1.78$ and $\langle P_2 \rangle_{bg} = 3.14$. This leads to the following selection cut:

$$0.5 < P_2 < 3.4 \ . \tag{3.5}$$

The other two parameters defining the lateral shower development are the leakage in η and ϕ directions:

$$P_3 = \frac{E_{37}^2 - E_{33}^2}{E_{37}^2} \qquad \text{and} \qquad P_4 = \frac{E_{77}^2 - E_{37}^2}{E_{77}^2} \ . \tag{3.6}$$

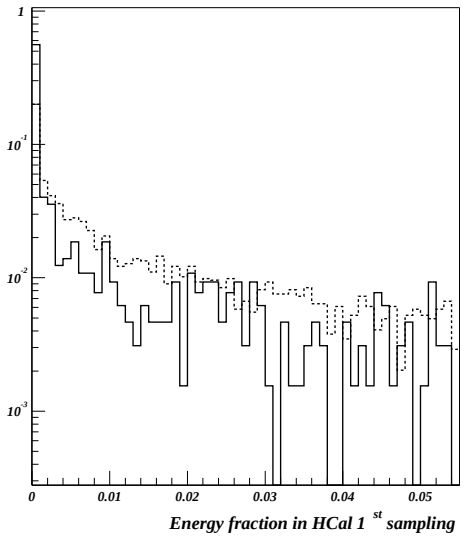

Figure 3: P_1*: Energy fraction in HCal first sampling.*

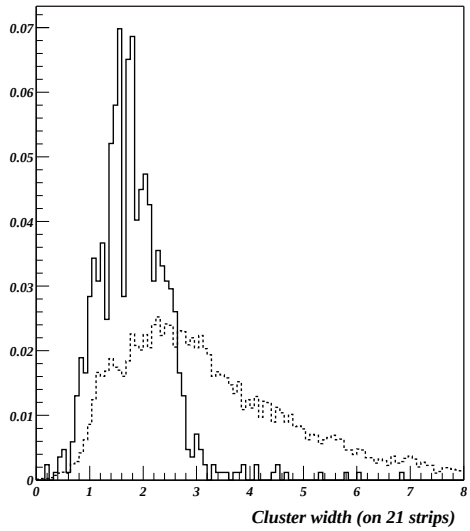

Figure 4: P_2*: Cluster width on 21 strips.*

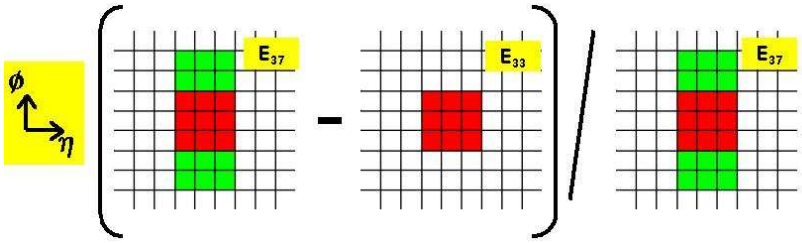

Figure 5: *The P_3 leakage variable definition. Each square represents an ECal middle cell.*

A definition of the leakage variable is shown on figure 5.

The P_3 and P_4 parameters are plotted on figures 6 and 7 and the extracted mean values for the signal and the background are:

$$\begin{cases} \langle P_3 \rangle_{signal} = 5.68\ \% \\ \langle P_4 \rangle_{signal} = 5.13\ \% \end{cases} \quad \text{and} \quad \begin{cases} \langle P_3 \rangle_{bg} = 16.57\ \% \\ \langle P_4 \rangle_{bg} = 19.96\ \% \end{cases} . \tag{3.7}$$

Therefore, we deduce the following selection criteria:

$$P_3 < 15\ \% \qquad \text{and} \qquad P_4 < 14\ \% . \tag{3.8}$$

The P_1-P_4 parameters provide a set of reasonable cuts for a clean photon identification. However, a non-negligible hadronic background, due mainly to neutral pions, will remain.

Neutral pions decay into two photons producing two maxima in the highly segmented ECal first sampling. The γ/π^0 rejection is thus based on the identification of a second maximum in ECal strips. Two new parameters are therefore defined:

$$P_5 = \frac{E^2_{max}}{E_{strips}} \qquad \text{and} \qquad P_6 = \frac{E^d_{max}}{E_{strips}} . \tag{3.9}$$

The P_5 parameter is related to the second maximum and the P_6 gives its significance. They are defined on figures 8 and the distributions are plotted on figure 9 and 10 for both signal and background. The mean values of the distributions are:

$$\begin{cases} \langle P_5 \rangle_{signal} = 3.67\ \% \\ \langle P_6 \rangle_{signal} = 2.70\ \% \end{cases} \quad \text{and} \quad \begin{cases} \langle P_5 \rangle_{background} = 11.58\ \% \\ \langle P_6 \rangle_{background} = 10.02\ \% \end{cases} \tag{3.10}$$

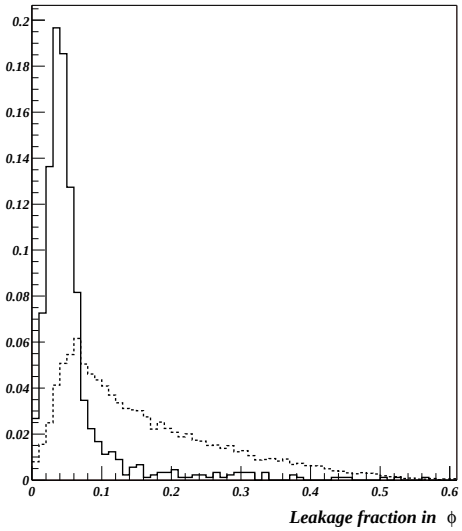

Figure 6: P_3: *Leakage in ϕ direction for signal (full line) and background (dashed).*

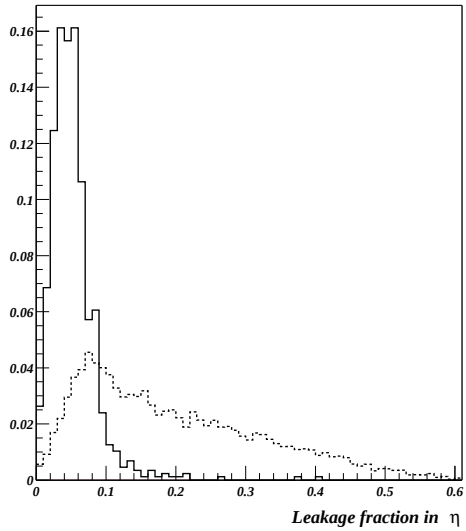

Figure 7: P_4: *Leakage in η direction for signal (full line) and background (dashed).*

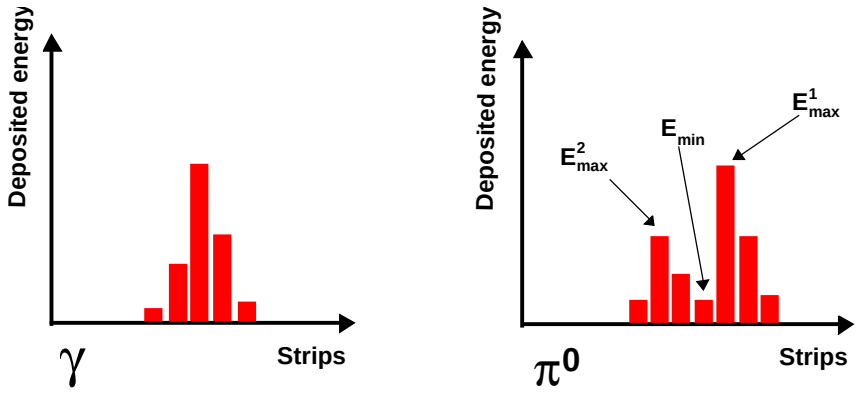

Figure 8: *Parameters defining the selection criteria for the γ/π^0. E^d_{max} is defined as follows: $E^d_{max} = E^2_{max} - E_{min}$*

The optimal selection cuts are therefore determined as follows:

$$P_5 < 10\ \%\ \text{and}\ P_6 < 8\ \% \tag{3.11}$$

A previous study of γ/π^0 rejection [15] has shown that such cuts would provide, for 50 *GeV* photons and with a 90% photon efficiency, a rejection factor of the order of 3. Combined testbeam photon data will soon allow to analyze γ/π^0 rejection in a large photon energy range, but it is clear that the π^0 background will not be completely suppressed at LVL2.

However, a good γ/π^0 identification will be primordial only at offline analysis level, in order to reject for example $B_d \to K^{*0}\pi^0$. In this case, other cuts could be applied (see for example in [16]), thus providing a good rejection factor.

3.2.2 Track pairs search in the inner detector

First, we reconstruct the tracks contained in the ROI defined previously. Tracks with transverse momentum[2] lower than 1 GeV/c are not considered. Reconstructed tracks are then separated into two groups; negatively charged tracks in the group **a** and positively charged tracks in the

[2]Computed in the laboratory frame.

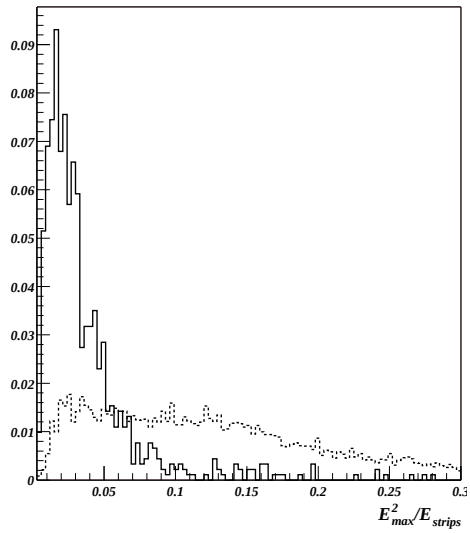

Figure 9: *Second maximum energy fraction in the strips (P_5)*

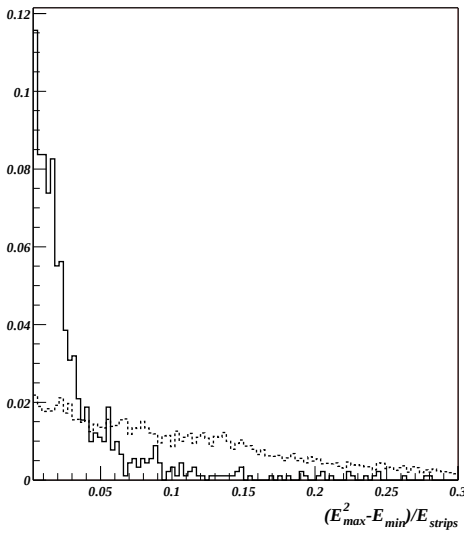

Figure 10: *Valley depth between the two maxima (P_6).*

group **b**. Hence we start with the following selection criteria (labelled V_i):

$$\begin{cases} V_1: \ p_T^a > 1 \ GeV \\ V_2: \ p_T^b > 1 \ GeV \\ V_3: \ Charge^a \times Charge^b = -1 \end{cases} . \tag{3.12}$$

Once the two groups are formed, and if there is at least one track in each group, we look for interesting track pairs, i.e. tracks coming from $K^{*0}(\phi)$ decay.

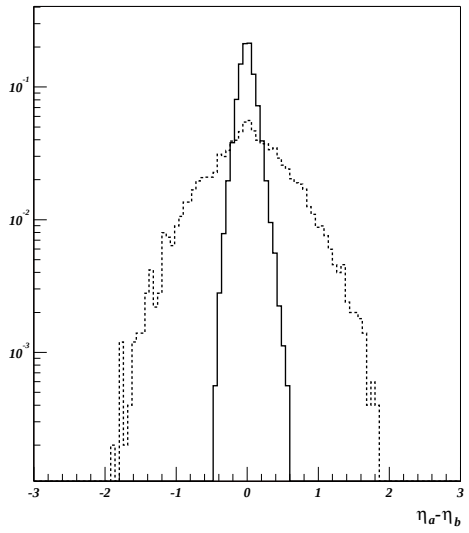

Figure 11: $\eta_a - \eta_b$. *Full line is for signal, dashed line for background.*

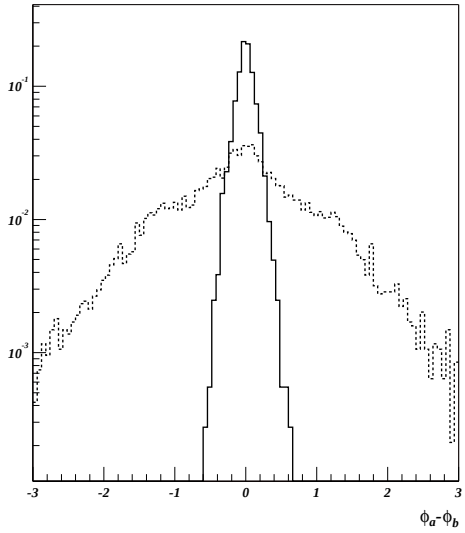

Figure 12: $\phi_a - \phi_b$. *Full line is for signal, dashed line for background.*

As shown on figs 11 and 12, the opening angle between these two tracks is relatively small compared to the background. Therefore we set the following cuts on the parameters[3] $\phi_a - \phi_b$ and $\eta_a - \eta_b$:

$$\begin{cases} V_4: |\phi_a - \phi_b| < \ 0.3 \ rad \\ V_5: |\eta_a - \eta_b| < \ 0.3 \end{cases} . \tag{3.13}$$

The selection process after V_4 and V_5 is presented on figure 13. Three different mass calculation are successively performed, in order to separate ϕ from K^{*0} hypothesis.

[3]Parameters discussed here are estimated at the vertex.

First mass calculation concerns ϕ, kaon masses are assigned to the two tracks, and invariant mass of the two tracks is calculated. If this mass corresponds to ϕ's one (within a 20 MeV mass window), further cuts, described later, are applied. Otherwise, the $K^{*0} \to K^+\pi^-$ option is tested, and then finally, if the event is still rejected, the $K^{*0} \to K^-\pi^+$. If no mass cut is passed, event is definitely rejected.

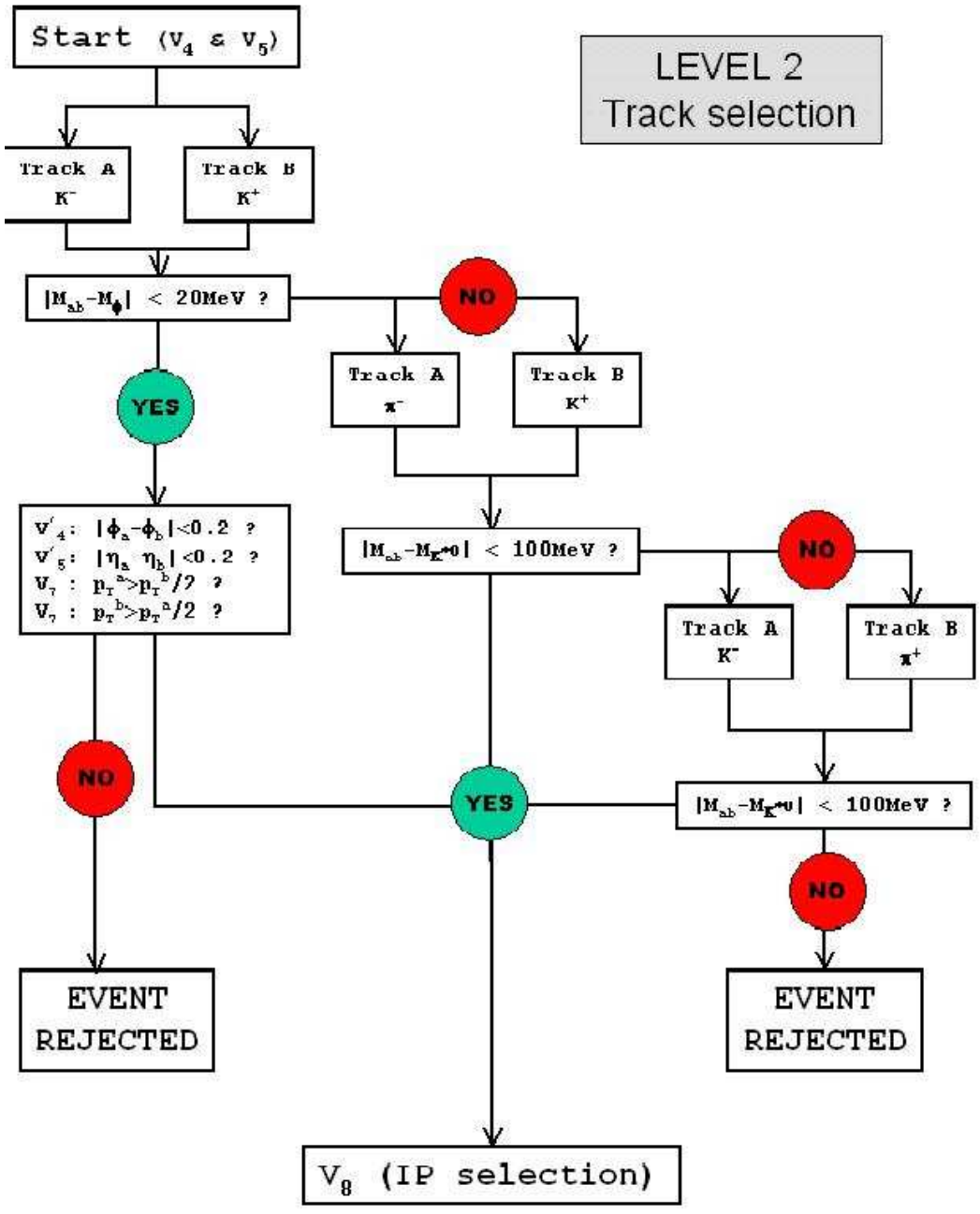

Figure 13: *The track selection process at level 2, between V_5 and V_8.*

If one of the three mass cuts is passed, selection on the transverse momentum distribution of the decay products is performed. These distributions are shown on figures 14, 15 and 16. We observe large differences between the signal and the background, particularly for the ϕ decay. The difference is smaller for the K^{*0}, as its decay products have different masses. In addition, it would be difficult to distinguish online $K^{*0} \to K^+\pi^-$ from $K^{*0} \to K^-\pi^+$ decay. Consequently the selection process is identical for these two decays.

Taking into account these remarks, cut V_7, depending on the decay, is defined. It is described in table 4, with the corresponding mass cut V_6. As it is shown on figure 13, V_4 and V_5 are slightly

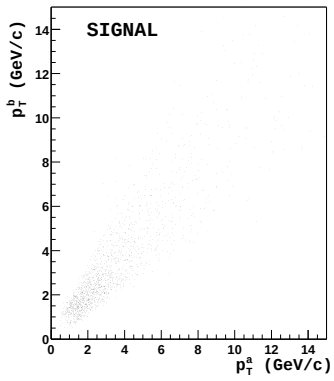

Figure 14: *Transverse momentum of the two tracks: $B_s \to \phi\gamma$ signal.*

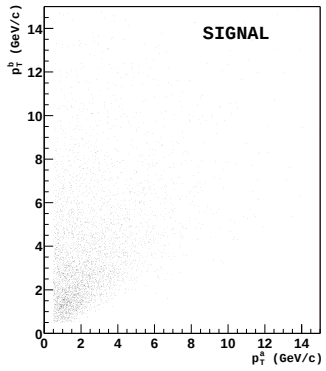

Figure 15: *Transverse momentum of the two tracks: $B_d \to K^{*0}_{K^+\pi^-}\gamma$ signal.*

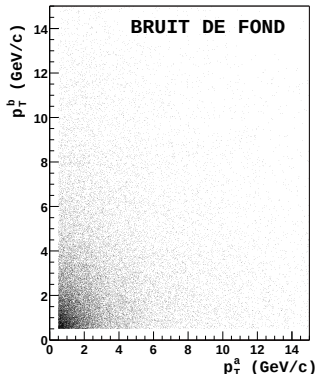

Figure 16: *Transverse momentum of the two tracks: background.*

Decay	V_6	V_7
$\phi \to K^+K^-$	$\lvert M_{ab} - M_\phi \rvert < 20\ MeV/c^2$	$p_T^a > \frac{1}{2}p_T^b$ and $p_T^b > \frac{1}{2}p_T^a$
$K^{*0} \to K^+\pi^-$ $K^{*0} \to K^-\pi^+$	$\lvert M_{ab} - M_{K^{*0}} \rvert < 100\ MeV/c^2$	$p_T^b > 2\ GeV/c$ or $p_T^a > 2\ GeV/c$

Table 4: *Definition of the selection cuts V_6 to V_7.*

modified in ϕ case. Indeed the opening angle between the two tracks is smaller in this case.

Then, events passing trough those cuts have to satisfy a selection involving the impact parameter.

As we consider that $K^{*0}(\phi)$ and B decay vertices are identical (because of $K^{*0}(\phi)$ very short lifetime), the tracks we are looking for are issued from a displaced vertex. Consequently their respective impact parameters should be larger than for the background tracks, these latter are in general issued from the primary vertex. In addition, the two tracks are kinematically very similar. Thus their impact parameters should be similar too.

This means that the tracks a and b should have, in most of the cases, the same impact parameter sign. This property is clearly verified on figure 17, where the product of the two impact parameters is plotted. As expected, we observe a symmetric distribution for the background, and a shifted one for the signal. However, a direct cut on the value of this product would affect B meson mean proper time measurement. We thus define the following selection criteria, which are not biasing proper time parameters:

$$V_8 : A_0^{track_a} \times A_0^{track_b} > 0 \quad \text{or} \quad |A_0^{track_a} - A_0^{track_b}| < 250\ \mu m. \tag{3.14}$$

In case of a negative value for the product, the pair is selected only if the two impact parameters are close.

3.2.3 Summary of the LVL2 study

The reconstruction efficiencies obtained for the different event samples, after all the applied LVL2 cuts, are summarized in table 5.

The trigger rate was estimated using the following formula:

$$N_{L_i} = \epsilon_{L_i} \times N_{background} = \epsilon_{L_i} \times \sigma_{bg} \times \mathcal{L}_{inst}\ , \tag{3.15}$$

where $\mathcal{L}_{inst} = 2 \times 10^{33} cm^{-2} s^{-1}$ and σ_{bg} is the global cross-section estimated in section 2.2.

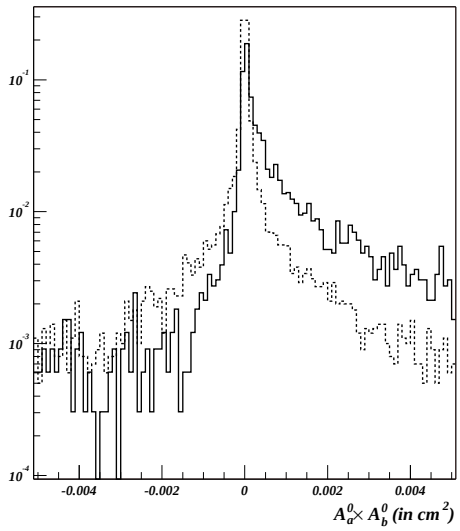

Figure 17: *The product of the two tracks impact parameter for the signal (full-black) and the background (dashed).*

Type	Background	$B_s \to \phi\gamma$	$B_d \to K^{*0}\gamma$
MC events	37796	14235	26807
After LVL2	188	938	1439
ϵ_{L_2} *(in %)*	$\mathbf{0.50 \pm 0.04}$	$\mathbf{6.6 \pm 0.2}$	$\mathbf{5.4 \pm 0.1}$

Table 5: *Comparison of the efficiencies after LVL2.*

On figures 18 and 19 are plotted the trigger rates at different levels (1 and 2) as a function of the LVL1 muon momentum threshold and the ECal ROI E_T threshold. The table 6 shows the values obtained for these rates, for the minimal thresholds defined in section 3.1.

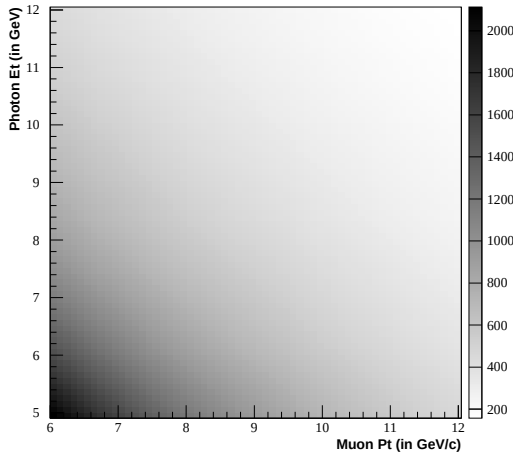

Figure 18: *Trigger rate after LVL1 (in Hz)*

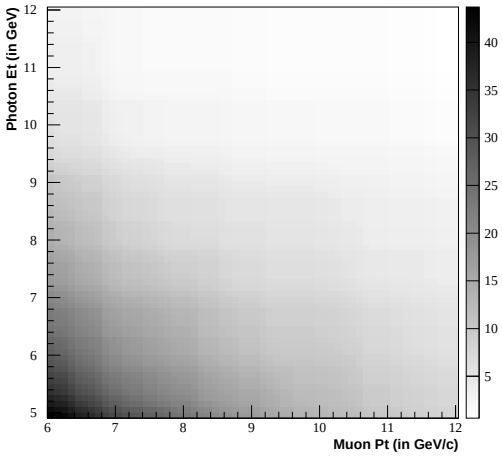

Figure 19: *Trigger rate after LVL2 (in Hz)*

The flexibility of the thresholds (p_T, E_T, etc...) is an important feature of the present study. Thresholds values can be slightly increased without affecting too much the physics reach. The next subsection will demonstrate this assessment.

N_{L_1} (in Hz)	$\mathbf{2150 \pm 20}$
N_{L_2} (in Hz)	$\mathbf{45 \pm 3}$

Table 6: *Maximum trigger rates after LVL1 and LVL2 at* $2 \times 10^{33}\mathrm{cm}^{-2}\mathrm{s}^{-1}$ *luminosity.*

3.3 Level 3

At LVL3 (Event Filter), one is able to propose a specific trigger scheme for each decay study. We introduce two labels as follows:

- $\boldsymbol{EF_{K\gamma}}$: dedicated to $B_d \to K^{*0}\gamma$.
- $\boldsymbol{EF_{P\gamma}}$: dedicated to $B_s \to \phi\gamma$.

This separation was prepared at LVL2. Indeed, an event passing LVL2 trough the ϕ mass selection will be directly assigned to $\boldsymbol{EF_{P\gamma}}$, and to $\boldsymbol{EF_{K\gamma}}$ if it passes the K^{*0} mass selection.

However, the difference with LVL2 is that we can refine the ID analysis, particularly on the reconstructed $K^{*0}(\phi)$ decay vertex.

The CTVMFT [17] vertexing routine is used to this end. This routine gives the following information on the fitted vertex:

- χ^2: χ^2/dof value.
- (x, y, z): vertex coordinates.
- $p = (p_x, p_y, p_z)$: $K^{*0}(\phi)$ candidate momentum.
- E: $K^{*0}(\phi)$ candidate energy.

The invariant mass of the candidate is calculated once we have passed the quality cut on the vertex which is $\chi^2/dof < 4$. This mass, computed using fitted track parameters, is of course more precise than the one calculated at LVL2. The following selection criteria are applied to $K^{*0}(\phi)$ meson candidate:

$$\begin{array}{c} 0.79\ GeV/c^2 < m_{K^{*0}} < 0.99\ GeV/c^2\ (\boldsymbol{EF_{K\gamma}}) \\ 1.00\ GeV/c^2 < m_{\phi} < 1.04\ GeV/c^2\ (\boldsymbol{EF_{P\gamma}}) \end{array} \quad . \tag{3.16}$$

A cut on vertex transverse length is then performed. As shown on figure 19, a significant part of the background could be rejected using a simple cut: $L_{tr}(B_{s,d}) > 250\ \mu m$.

For the B meson, a loose mass cut is applied:

$$4.7\ GeV/c^2 < m_{B_{s,d}} < 6.0\ GeV/c^2 \quad . \tag{3.17}$$

Efficiencies obtained after performing these cuts are summarized in table 7.

This efficiency leads to the following trigger rates:

$$N_{L3}^{\boldsymbol{EF_{P\gamma}}} \approx 1.0 \pm 0.5 Hz \qquad and \qquad N_{L3}^{\boldsymbol{EF_{K\gamma}}} \approx 1.2 \pm 0.5 Hz\ . \tag{3.18}$$

which are in good agreement with our requirements. These cuts are largely sufficient to ensure very low output rates. Therefore, and in order to maximize the number of staged events, we will keep some other cuts for further analysis.

Using the cross sections determined in section 2, it is straight forward to evaluate the number of triggered signal events. We obtain:

$$\begin{array}{c} N_{B_s \to \phi\gamma} \approx 158 \pm 16\ events/fb^{-1} \\ N_{B_d \to K^{*0}\gamma} \approx 469 \pm 41\ events/fb^{-1}. \end{array} \tag{3.19}$$

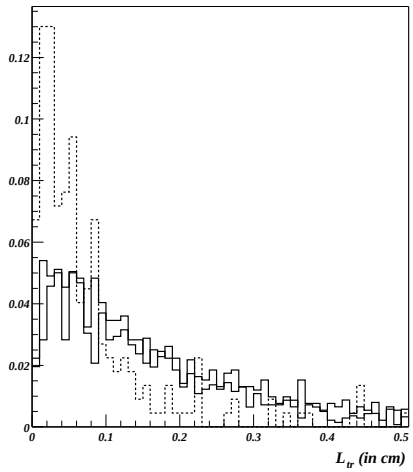

Figure 20: *Transverse length distribution at level 3: dashed line is for the background, full lines for the different signals.*

	$\boldsymbol{EF_{P\gamma}}$		$\boldsymbol{EF_{K\gamma}}$	
Type	Background	Signal	Background	Signal
Before LVL1	37796	14235	37796	26807
After LVL3	4	754	5	1021
ϵ_{L_3} *(in %)*	$\mathbf{0.011 \pm 0.005}$	$\mathbf{5.3 \pm 0.2}$	$\mathbf{0.013 \pm 0.006}$	$\mathbf{3.8 \pm 0.1}$

Table 7: *Compared efficiencies after LVL3 for the different schemes (numbers refer to MC events).*

For $\approx 20\ fb^{-1}$ (1 year at low luminosity), we get:

$$\begin{array}{c} N_{B_s \to \phi\gamma} \approx 3160 \pm 320\ events \\ N_{B_d \to K^{*0}\gamma} \approx 9380 \pm 820\ events. \end{array} \tag{3.20}$$

These values are obtained with the minimal thresholds, i.e. $E_T^{ROI} > 5\ GeV$ and $p_T^{tracks} > 1\ GeV/c$. They are to be compared to the LHCb expectation for the same running period, i.e. 9300 $B_s \to \phi\gamma$ and 35000 $B_d \to K^{*0}\gamma$ [16]. The positive aspect of ATLAS events is that muon is present in each of them. This muon can be used for B flavor tagging, which is required in $\mathcal{C}P$ violation measurements.

However, we have shown the most optimistic expectation and it will be perhaps necessary, because of bandwidth constraints requirements, to raise the trigger thresholds.

Figures 21 and 22 gives an estimate of the triggered events for different threshold values of p_T^{γ}. The different distributions correspond to different p_T^{tracks} thresholds, from 1 to 3 GeV/c. These values could be compared to the CDF experiment estimate of about 60 $B_s \to \phi\gamma$ events and 180 $B_d \to K^{*0}\gamma$ events within 2 fb^{-1} (Run II integrated luminosity) [18].

The number of expected $B_d \to K^{*0}\gamma$ events at B-factories (BaBar and BELLE) at the end of the running period is about 1000 events for each experiment. It becomes clear that ATLAS will be very competitive with current experiments, and will also allow an interesting crosscheck with LHCb results.

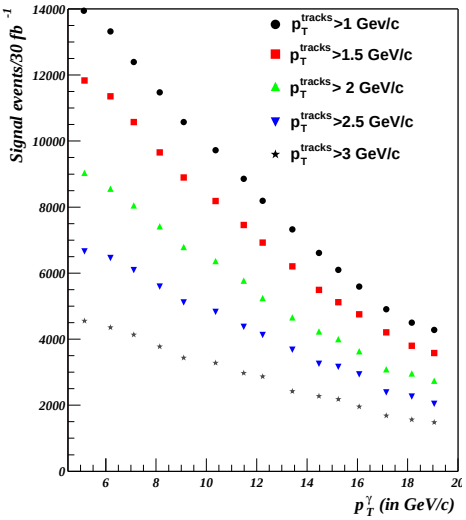

Figure 21: *Reconstructed* $B_s \rightarrow \phi\gamma$ *events for* 30 fb^{-1}

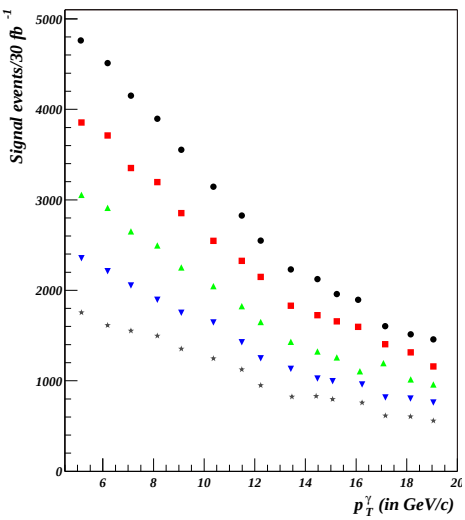

Figure 22: *Reconstructed* $B_d \rightarrow K^{*0}\gamma$ *events for* 30 fb^{-1}

3.4 Summary of the radiative B decay selection

Here is a summary of all the steps and selections we have performed in order to get radiative penguins events:

- At **LEVEL 1** we take a muon with a $p_T > 6\ GeV/c$ in the spectrometer, and an isolated ROI with ($E_T > 5\ GeV$) in the electromagnetic calorimeter.
- At **LEVEL 2** we perform a photon identification in the ECal and analyze the ID ROI. We only reconstruct the tracks with $p_T > 1\ GeV/c$, and group the tracks as a function of their charge. Then, we look for the interesting track pairs. At this step, different mass combinations are tested, in order to choose between ϕ and K^{*0} hypothesis.
- At **LEVEL 3** we perform the event reconstruction, mass cuts, vertexing, displaced vertex cut, and we define specific trigger schemes for each channel: $\boldsymbol{EF_{K\gamma}}$ for $B_d \rightarrow K^{*0}\gamma$ and $\boldsymbol{EF_{P\gamma}}$ for $B_s \rightarrow \phi\gamma$.

Table 8 gives the maximum output rates for the two strategies which have been studied.

Type	$\boldsymbol{EF_{K\gamma}}$	$\boldsymbol{EF_{P\gamma}}$
N_{LVL1} *(in Hz)*	$\mathbf{2150 \pm 20}$	
N_{LVL2} *(in Hz)*	$\mathbf{45 \pm 3}$	
N_{LVL3} *(in Hz)*	$\mathbf{1.2 \pm 0.5}$	$\mathbf{1.0 \pm 0.5}$

Table 8: *Summary of the different trigger rates obtained with the minimal thresholds.*

If necessary, values presented in this table can be slightly lowered using higher thresholds. But even with higher thresholds, the number of reconstructed signal events in ATLAS will be significantly larger than the existing/expected results of CDF and B factories.

4 The significance estimate

The significance is defined to be the ratio of the signal to the squared background for a given running period:

$$\frac{S}{\sqrt{B}} = \sqrt{S} \times \sqrt{\frac{S}{B}} = \begin{cases} (0.156 \pm 0.004) \times \sqrt{\epsilon_{signal}} \times \sqrt{\frac{S}{B}} \times \sqrt{\int \frac{\mathcal{L}_{inst}}{2\times 10^{33}} dt} & (B_d \to K^{*0}\gamma) \\ (0.077 \pm 0.002) \times \sqrt{\epsilon_{signal}} \times \sqrt{\frac{S}{B}} \times \sqrt{\int \frac{\mathcal{L}_{inst}}{2\times 10^{33}} dt} & (B_s \to \phi\gamma) \end{cases} . \tag{4.1}$$

Our background sample was not sufficient to develop a complete offline analysis. Indeed such a study will require several millions of background events and the production of specific events such as $B_d \to K^{*0}\pi^0$. However, 40000 background events were enough to perform a preliminary estimate of the significance.

The background suppression can be performed at different steps, the first one is to improve $K^{*0}(\phi)$ identification in the ID. The reconstructed $K^{*0}(\phi)$ mesons are plotted on figures 23 and 24. The plain plots show the good events, identified at the reconstruction level by the "truth" variable. Open lines distributions show all the reconstructed event. The purity of the different signals, defined as: $\rho = \frac{Evts^{true}}{Evts^{reconstructed}}$, is summarized in table 9.

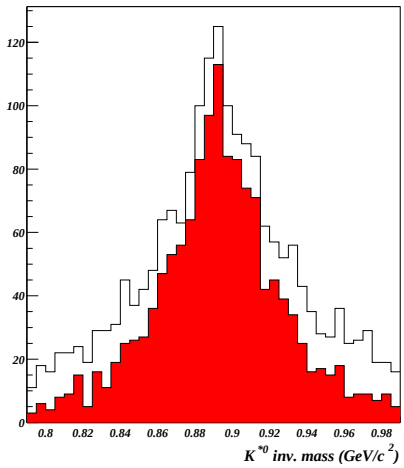

Figure 23: *Reconstructed* K^{*0}

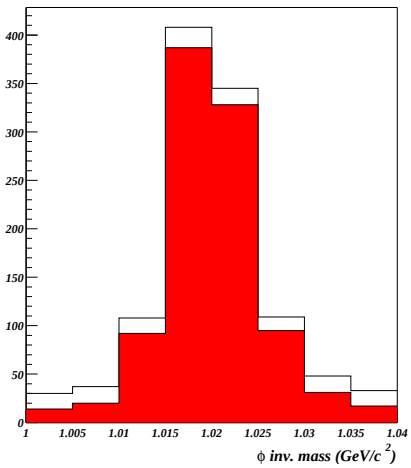

Figure 24: *Reconstructed* ϕ

ρ_ϕ (in %)	**86.8 ± 1.0**
$\rho_{K^{*0}}$ (in %)	**73.2 ± 1.1**

Table 9: *Purity of the signal in ID at level 3.*

The results of table 9 confirm that ϕ signal is easier to reconstruct than K^{*0} one. For the background, we select after event filter 96 events in the inner detector. Therefore, we have a reasonable statistic to deal with and to use for testing our event selection.

Improving the $K^{*0}(\phi)$ purity can be done using the impact parameter significance and the isolation of B meson.

The impact parameter significance is defined as:

$$SIP(A_0) = \frac{A_0}{\sigma_{A_0}} , \tag{4.2}$$

where A_0 is the impact parameter of the track and σ_{A_0} the error on A_0. This parameter should be larger for the signal tracks (issued from displaced vertex) than for the background ones. This

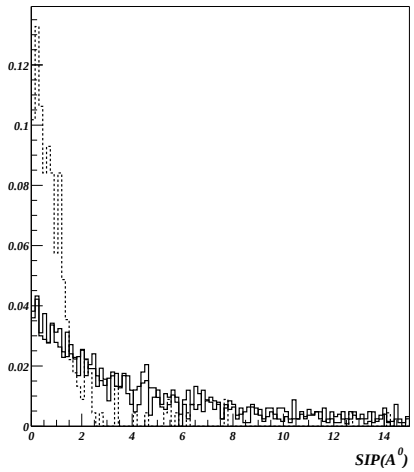

Figure 25: *Impact parameter significance after level 3: dashed line is for the background, full lines for the different signals.*

effect is clearly observable on figure 25. We can use the cut $SIP(A_0) > 1$ in order to reject most of the background tracks.

It has been demonstrated that B hadrons carry most of the originating b quark energy [19]. The consequence of this property is the B hadron isolation. This property is measured using a cone whose vertex is exactly the B decay vertex. The isolation criteria is thus easy to define:

$$Isol(B) = \frac{p_T^B}{p_T^B + \sum\limits_{\substack{i \in cone \\ i \notin B}} p_T^i} \ . \tag{4.3}$$

If the selected track pair is isolated, the isolation criteria value should reach the value 1.

The transverse momentum of the reconstructed tracks constituting the cone are selected if $p_T^i > 0.5\ GeV/c$. The cone is defined around the direction of the $K^{*0}(\phi)$ mesons.

On figure 26 is plotted the isolation criteria for the different event types. As expected, the signal events distributions are peaked to 1.

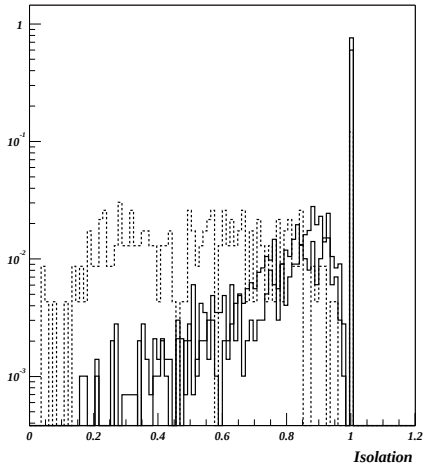

Figure 26: *Isolation parameter after LVL3: dashed line for the background, full lines for the different signals.*

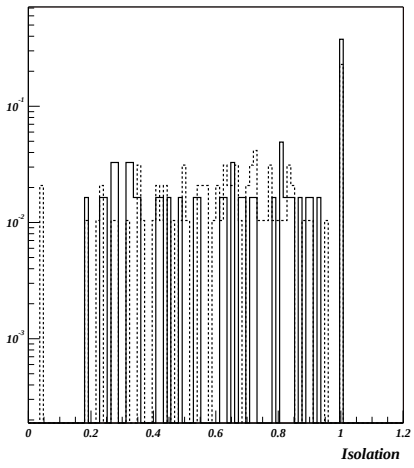

Figure 27: *Isolation parameter for the background with (dashed) and without (full-line) the pile-up*

On figure 27 are plotted the isolation parameter for the background with and without pile-up respectively. It has to be noticed that this parameter does not show a dependency on the pile-up

at low luminosity. This will allow us to use this cut on the signal when it will be studied with the pile-up:

$$Isol = \frac{p_T^{K^{*0}(\phi)}}{p_T^{K^{*0}(\phi)} + \sum\limits_{i \notin K^{*0}(\phi)}^{i \in cone} p_T^i} > 0.7 \ . \tag{4.4}$$

4.1 Summary of the results

When all the selection criteria defined previously are applied, we obtain new 'clean' results presented in table 10. The purity of the signal is clearly improved. As shown in table 11, the loss in the signal reconstruction efficiency is of the order of 30% which is small compared to the gain in background suppression. Indeed, the background in the inner detector goes from 82 to 11 events, giving a rejection factor of 7.5. It is also interesting to notice that at the B meson level, no event remain.

ρ_ϕ (in %)	$\mathbf{97.3 \pm 0.6}$
$\rho_{K^{*0}}$ (in %)	$\mathbf{96.5 \pm 0.6}$

Table 10: *Signal purity in the ID after offline cuts.*

Type	$B_d \to K^{*0}\gamma$	$B_s \to \phi\gamma$
ϵ_{L3}^{signal} (in %)	$\mathbf{3.8 \pm 0.1}$	$\mathbf{5.3 \pm 0.2}$
$\epsilon_{after}^{signal}$ (en %)	$\mathbf{2.6 \pm 0.1}$	$\mathbf{3.7 \pm 0.2}$
$\frac{\epsilon_{after}^{signal}}{\epsilon_{L3}^{signal}}$	$\mathbf{0.68 \pm 0.02}$	$\mathbf{0.69 \pm 0.02}$

Table 11: *Effect of offline cuts on the reconstruction efficiency.*

The signal to background ratio is given by:

$$\left(\frac{S}{B}\right)_{after} = \frac{\epsilon_{after}^{signal}}{\epsilon_{LVL3}^{signal}} \frac{\epsilon_{LVL3}^{bg}}{\epsilon_{after}^{bg}} \left(\frac{S}{B}\right)_{LVL3} \ , \tag{4.5}$$

and the calculated values are found in table 12. As shown, the signal to background ratio has been improved from 10^{-7} before LVL1 to nearly 10^{-2} after preliminary offline cuts. In addition, these preliminary value can be slightly improved in future analysis if more statistics is available for the background sample.

Type	$B_d \to K^{*0}\gamma$	$B_s \to \phi\gamma$
$\left(\frac{S}{B}\right)_{L3}$ (in %)	$\mathbf{\approx 0.10}$	$\mathbf{\approx 0.03}$
$\left(\frac{S}{B}\right)_{after}$ (in %)	$\mathbf{\approx 0.47}$	$\mathbf{\approx 0.17}$

Table 12: *Signal to background ratio after the ID cuts.*

On figures 28 and 29 are plotted the significance estimates as a function of $\frac{S}{B}$ and the integrated luminosity. The efficiencies values ϵ_{signal} used to compute the significance are those

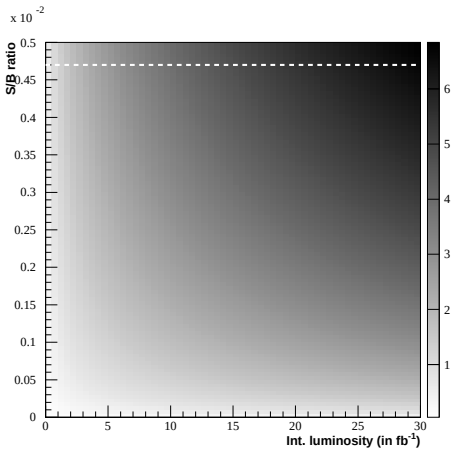

Figure 28: $\frac{S}{\sqrt{B}}$ *vs* $\frac{S}{B}$ *and integrated luminosity for* $B_d \to K^{*0}\gamma$.

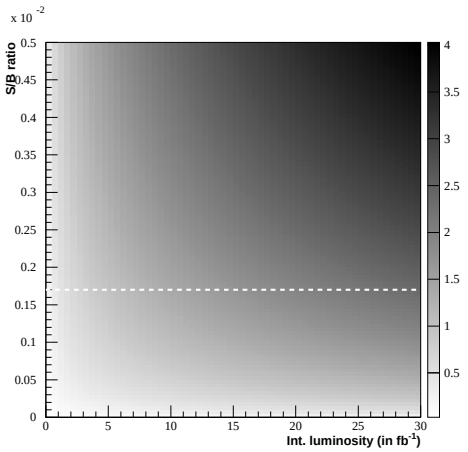

Figure 29: $\frac{S}{\sqrt{B}}$ *vs* $\frac{S}{B}$ *and integrated luminosity for* $B_s \to \phi\gamma$.

indicated in table 8. A dashed line on each plot shows the preliminary signal to background value presented in 12.

We can reasonably expect to obtain $\frac{S}{B}$ far better than one percent. And we see on figs 28 and 29 that one year at low luminosity with a $\frac{S}{B} = 0.5$ % leads to significance larger than 4. With our preliminary estimates, which use very pessimistic lower limits, we have already significance values of 5 for $B_d \to K^{*0}\gamma$, and 2 for $B_s \to \phi\gamma$ with 20 fb^{-1}. This result is a guarantee for observing radiative B decays in ATLAS even for a very short data taking period.

5 Conclusion and perspectives

A trigger scheme to study radiative B decays in ATLAS has been presented. The number of triggered events after one year at luminosity 2×10^{33} cm^{-2} s^{-1} will be of the order of 9400 and 3200 signal events for $B_d \to K^{*0}\gamma$ and $B_s \to \phi\gamma$ respectively. We can expect to keep about 70 % of these events after the offline selection, with signal to noise ratio of the order of at least 10^{-2}. The proposed strategy should now be tested using realistic trigger simulation. Qualitative arguments presented in section 3.1 should be checked using LVL1 calorimeter trigger software. The possibility to perform LVL2 calorimeter analysis before LVL2 inner detector analysis should be also tested, in order to allow best photon candidate selection.

Better signal to background ratios can be reached if a complete offline analysis is performed, which was not discussed here because of too low background statistics (A precise offline analysis requires at least 3×10^6 background events).

However, preliminary significance estimates already show very encouraging results. ATLAS should be able to obtain clear radiative B decay signals after one year at low luminosity, thus allowing precise branching ratio measurement and useful crosscheck with LHCb results, in particular for $B_s \to \phi\gamma$. This latter mode will certainly be discovered only at LHC.

References

[1] A.L. Kagan et M. Neubert - *"Isospin Breaking in $B \to K^*\gamma$ Decays"* - Phys.Lett. B539(2002), 227

[2] A.L. Kagan et M. Neubert - *"Direct $\mathcal{CP}$ Violation in $B \to X_s\gamma$ Decays as a Signature of New Physics"* - Phys.Rev. D58(1998), 094012

[3] R. Ammar *et al.* [CLEO Collaboration] - *"Evidence for penguins: first observation of $B \to K^*(892)\gamma$"* - Phy.Rev.Lett. 71(1993), 674

[4] M. Nakao - *"Radiative and Electroweak Rare B Decays"* - hep-ex/0312041 - (2003)

[5] R. Sturrok *et al.* - *"A Step Towards A Computing Grid For The LHC Experiments: ATLAS Data Challenge 1"* - CERN-PH-EP-2004-028 - (2004)

[6] T. Sjöstrand *et al.* - *"Pythia 6.2: Physics and Manual"* - hep-ph/0108264 - (2001)

[7] M. Smizanska - *"PythiaB: an interface to Pythia6 dedicated to the simulation of beauty events"* - ATL-COM-PHYS-2003-038 - (2003)

[8] "Level 1 Trigger TDR" LHCC-98-14

[9] Collectif - *"ATLAS High-Level Trigger, Data Acquisition and Controls"* - ATLAS TDR-016 - (2003)

[10] N. Nikitin - *Private communication*

[11] S. Viret - *"Radiative B decays with ATLAS"* - http://lpsc.in2p3.fr/atlas/Radiativ/

[12] S. Eidelman *et al.* (Particle Data Group) - *"Review of Particle Physics"* - Phys. Lett. B592(2004), 1

[13] K. Kordas - *"Search for Penguin Decays of B Mesons at* **CDF***"* - PhD Thesis: McGill University - (1999) - http://www-lib.fnal.gov/archive/thesis/fermilab-thesis-1999-16.shtml

[14] Collectif - *"ATLAS Technical Design Report Vol.2: Physics Performance"* - (1999)

[15] S. Saboumazrag - *"Réalisation du pré-échantillonneur central d'ATLAS et étude de la séparation gamma / pi0 dans le calorimètre électromagnétique"* - PhD Thesis: Joseph Fourier University - (2004) - http://tel.ccsd.cnrs.fr/documents/archives0/00/00/53/97/index_fr.html

[16] G. Pakhlova & I. Belyaev - *"Radiative B decays with LHCb"* - LHCb note 2003-090(2003)

[17] F.Tartarelli - *"Documentation for the CTVMFT vertex fitting package in ATLAS"* - http://tarta.home.cern.ch/tarta/vtx/docu.html

[18] K. Anikeev *et al.* -*"B physics at the Tevatron: run II and beyond"* - FERMILAB-Pub-01/197 (hep-ph/0201071) - (2001)

[19] J.D. Bjorken - *"Properties of Hadron Distributions in Reactions Containing Very Heavy Quarks"* - Phys.Rev. D17(1978), 171-173